Refractory–Slag–Metal–Inclusion Multiphase Reactions Modeling Using Computational Thermodynamics: Kinetic Model for Prediction of Inclusion Evolution in Molten Steel

JAE HONG SHIN, YONGSUG CHUNG, and JOO HYUN PARK

The refractory–slag–metal–inclusion multiphase reaction model was developed by integrating the refractory–slag, slag–metal, and metal–inclusion elementary reactions in order to predict the evolution of inclusions during the secondary refining processes. The mass transfer coefficient in the metal and slag phase, and the mass transfer coefficient of MgO in the slag were employed in the present multiphase reactions modeling. The ''Effective Equilibrium Reaction Zone (EERZ) Model'' was basically employed. In this model, the reaction zone volume per unit step for metal and slag phase, which is dependent on the 'effective reaction zone depth' in each phase, should be defined. Thus, we evaluated the effective reaction zone depth from the mass transfer coefficient in metal and slag phase at 1873 K (1600 °C) for the desulfurization reaction which was measured in the present study. Because the dissolution rate of MgO from the refractory to slag phase is one of the key factors affecting the slag composition, the mass transfer coefficient of MgO in the ladle slag was also experimentally determined. The calculated results for the variation of the composition of slag and molten steel as a function of reaction time were in good agreement with the experimental results. The $MgAl_2O_4$ spinel inclusion was observed at the early to middle stage of the reaction, whereas the liquid oxide inclusion was mainly observed at the final stage of the refining reaction. The content of CaO sharply increased, and the SiO_2 content increased mildly with the increasing reaction time, while the content of Al_2O_3 in the inclusion drastically decreased. Even though there is slight difference between the calculated and measured results, the refractory–slag–metal multiphase reaction model constructed in the present study exhibited a good predictability of the inclusion evolution during ladle refining process.

DOI: 10.1007/s11663-016-0734-6

I. INTRODUCTION

PERFORMANCE of steel products is significantly affected by the steel cleanliness. Especially, the $MgAl_2O_4$ spinel inclusion is very harmful because it causes the nozzle clogging as well as the surface defects in semi- and final products.[1–10] Hence, it is crucial to avoid the formation of spinel during the secondary refining process. The spinel inclusion is formed by the complicated slag–metal–refractory multiphase reactions during ladle refining process. Therefore, it is important to understand the complex multiphase reactions for controlling the spinel formation behavior.

The formation behavior or modification of spinel inclusion in molten steel has been investigated in the viewpoint of thermodynamics since 1980s.[1–15] Specifically, Park *et al.*[5–10] reported the formation mechanisms of spinel inclusion and the countermeasures during the stainless steel refining and casting processes. More recently, Verma *et al.*[12–14] reported the mechanism of calcium modification of alumina and spinel inclusions. These studies have been carried out based on the local equilibrium concept. If the slag–metal reaction reaches the universal (or global) equilibrium, the inclusion composition should be identical to slag composition. However, in the actual plant, the inclusion composition is different from the ladle slag composition. Moreover, the various chemical compositions of the inclusion have been observed, indicating that the chemical reactions occurred in the ladle do not reach an equilibrium state.

Therefore, in order to predict the formation behavior of inclusions during the ladle refining process, the process analysis not only based on the equilibrium study but also based on the kinetic study is necessary. Several kinetic models have been developed to predict the phenomena of metallurgical reactors.[15–29] Ding *et al.* developed a dynamic model to simulate the vacuum oxygen decarburization (VOD) process by

JAE HONG SHIN, Graduate Student, and JOO HYUN PARK, Professor, are with the Department of Materials Engineering, Hanyang University, Ansan 426-791, Korea. Contact e-mail: basicity@hanyang.ac.kr YONGSUG CHUNG, Professor, is with the Department of Advanced Materials Engineering, Korea Polytechnic University, Siheung 429-793, Korea.

Manuscript submitted January 25, 2016.
Article published online June 28, 2016.

employing a method based on a stepwise comparison of reaction free energies.[16]

A kinetic model for the RH degassing process was developed by Van Ende *et al.*[17] using the "Effective Equilibrium Reaction Zone (EERZ)" model in conjunction with FactSage™ software.[23,24] More recently, they developed a kinetic model for the continuous casting process.[18] A similar concept was accepted by Roy *et al.*[19,20] to evaluate the effect of silicon on the desulfurization rate of Al-killed steel. Kim developed the "Diffusion Coupled Reaction Zone" model, which combines EERZ model and coupled reaction model. The DCRZ model was applied to predict the changes in the composition of mold flux for continuous casting of high-Al-containing steels.[21]

The kinetic model for the ladle refining process has also been developed.[22–29] Graham and Irons developed the ladle metallurgy process model to describe the kinetics of coupled slag–metal reactions assuming that the rates were mixed transport controlled.[24] They found that the mass transfer capacity coefficient (a lumped parameter including the mass transfer coefficient, slag–metal interfacial area, and steel volume) increased with the increasing stirring power with the exponent of 1.4 and successfully predicted the changes in the composition of steel and slag during desulfurization reaction. However, the formation behavior of inclusion during the ladle refining process was not considered in this study.

Recently, Galindo *et al.*[25] developed a kinetic model based on the coupled reaction model to calculate the modification from alumina to spinel inclusion during the ladle refining process. Using this model, they predicted magnesium pick-up from ladle slag and calculated the increasing rate of magnesium content in the inclusions. Similar approach based on a coupled reaction model has also been employed by Harada *et al.*[26–28] to predict the changes in slag, metal, and inclusion composition as a function of reaction time. However, since they determined several model parameters to match the calculation results with plant operation or experimental results, these model parameters should be modified if the experimental conditions are changed.

Therefore, in order to predict the evolution of inclusions during the ladle refining process, the refractory–slag–metal–inclusion multiphase reaction model was developed by integrating the refractory–slag, slag–metal, and metal–inclusion elementary reactions. For the convenient and flexible extendibility of the present refractory–slag–metal–inclusion multiphase reaction model, only the effective reaction volume in the metal and slag phase, and the mass transfer coefficient of MgO in the slag were employed in the model. These values were directly measured in the present study. Finally, the effect of slag composition on the evolution process of inclusions was simulated using the refractory–slag–metal–inclusion multiphase reaction model developed in the present study.

II. EXPERIMENTAL

A. *Effect of Refractory–Slag–Metal Multiphase Reactions on Inclusion Formation Behavior in Molten Steel*

The Fe-0.8Mn-0.4Si-0.3C-0.05Al steel (mass pct) and 40CaO-27Al_2O_3-13SiO_2-10CaF_2-10MgO (mass pct) slag were reacted for 30 minutes at 1873 K (1600 °C) in a fused MgO crucible (60 mm OD × 52 mm ID × 120 mm H) with a graphite heater under an Ar-3 vol pct H_2 gas atmosphere using a high-frequency induction furnace as shown in Figure 1. The Fe-0.8Mn-0.2Si-0.3C steel was prepared using a vacuum induction melting furnace. The slag was premelted in a graphite crucible (50 mm OD × 44 mm ID × 88 mm H) for 2 hours in an electric resistance furnace under an inert atmosphere.

The temperature was controlled by a B-type thermocouple covered with an alumina sheath. After the temperature reached 1873 K (1600 °C), Fe-16 mass pct Al alloy which was prepared using an induction furnace was added into the Fe-Mn-Si-C melt under an inert atmosphere to control the initial Al content. The molten steel was maintained during 30 minutes for the homogenization of composition. The premelted slag (50 g) was then added through the quartz tube on the surface of molten steel (600 g). The moment of contact between slag and liquid steel was taken as the starting time of the refractory–slag–metal reaction. After a certain reaction period (5, 10, 15, and 30 minutes), the liquid steel and slag samples were quickly taken using quartz tube and steel rod, respectively, and then rapidly quenched by dipping into the brine.

After experiments, the steel samples were prepared for chemical analysis. The content of oxygen was determined using a combustion analyzer, and that of steel components was obtained using Inductively Coupled Plasma Atomic Emission Spectrometry (ICP-AES, ACROS, SPECTRO). An automatic feature analysis (AFA) system equipped in Scanning Electron Microscopy–Electron Dispersive Spectrometry (SEM-EDS, JSM-7800, JEOL) was employed to characterize the inclusions including chemistry, morphology, and population statistics. The accelerating voltage was 15 kV, and the detection limit of inclusion diameter was 1 μm. The slag composition was analyzed by an X-ray Fluorescence Spectrometry (XRF, S4 explorer, Bruker).

B. *Determination of Mass Transfer Coefficients in Metal and Slag Phases: Desulfurization Experiments*

The Fe-0.8Mn-0.4Si-0.3C-0.05Al (mass pct) steel sample (600g) was melted in the MgO crucible using a high-frequency induction furnace at 1873 K (1600 °C). After the steel sample was melted down, the sulfur content was initialized to 0.25 mass pct by adding iron sulfide (FeS) into the molten steel. The 40CaO-27Al_2O_3-13SiO_2-10CaF_2-10MgO (mass pct) slag (50 g) was then added to the melt surface. After a certain reaction period (5, 10, 15, and 30 minutes), the liquid steel and slag samples

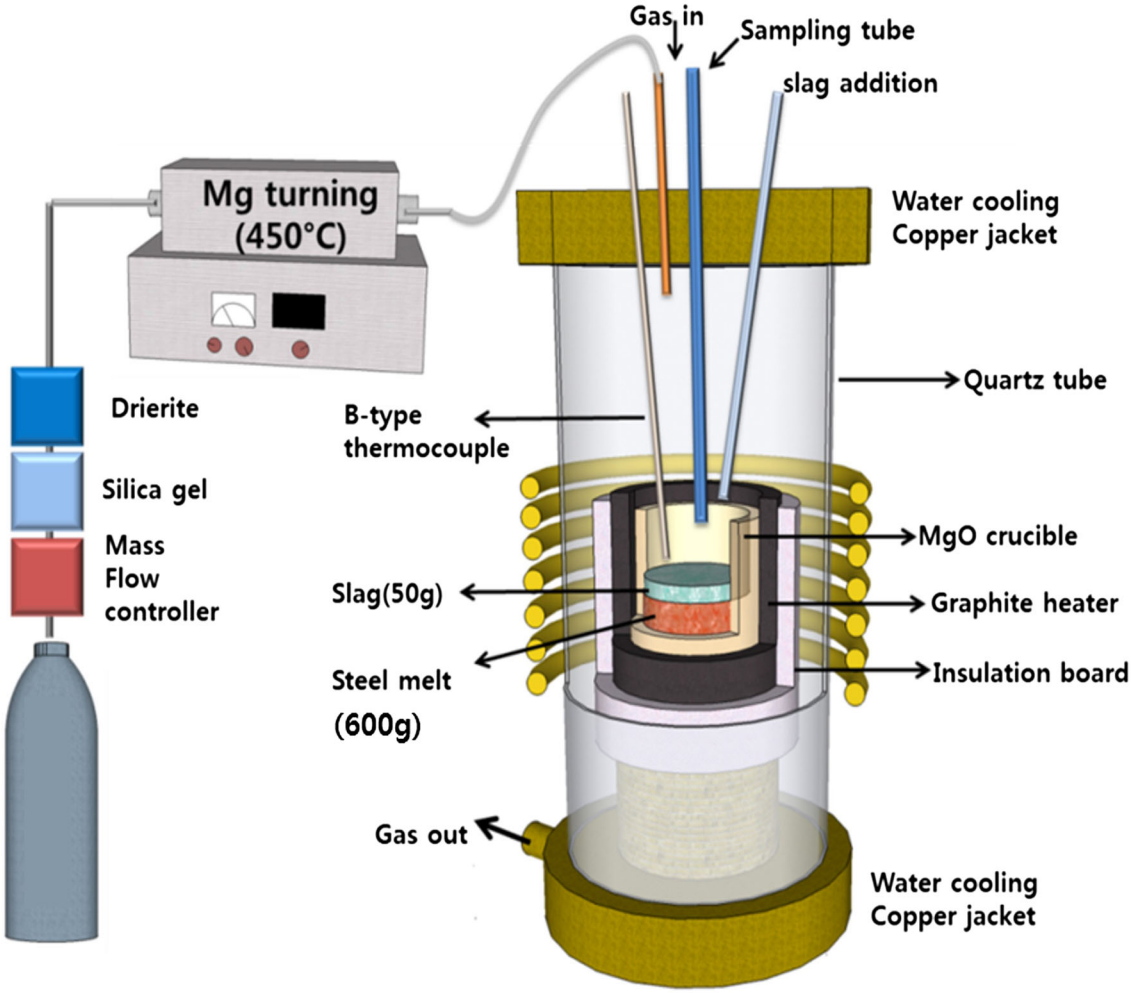

Fig. 1—Schematic diagram of the experimental apparatus.

were quickly taken using quartz tube and steel rod, respectively, and then rapidly quenched by dipping into brine. After experiments, the sulfur content in the steel and slag were measured using combustion Carbon/Sulfur analyzer (CS300, LECO).

C. *Dissolution Rate of MgO from Refractory to Slag Phase*

The Fe-0.8Mn (mass pct) steel (600 g) was melted in the MgO crucible using a high-frequency induction furnace at 1873 K (1600 °C). After steel sample was melted down, the CaO-Al_2O_3-SiO_2-CaF_2-MgO system slag (50 g) was then added to the melt surface. After a certain reaction period (5, 15, 30, and 90 minutes), the slag sample was quickly taken by dipping steel rod into the slag layer and then rapidly quenched by dipping into the brine. After experiments, the slag composition was analyzed by an XRF spectrometry.

III. CONCEPT OF CALCULATION

A. *Effective Equilibrium Reaction Zone (EERZ) Model*

In the present study, the following reactions are considered to predict the formation behavior of inclusion during the refractory–slag–metal multiphase reactions:

R1 Reaction between molten steel and slag;
R2 Dissolution of the refractory into the slag; and
R3 Evolution of the inclusions in molten steel, which was varied by R1 and R2.

According to R1, the oxidation–reduction reaction occurs at the slag–metal reaction zone, resulting in the variation of the chemical composition of molten steel including the oxygen potential at slag–metal interface. Dissolution of MgO from the refractory into the slag (R2) is also considered because the slag composition, which was changed by MgO pick-up, can affect the chemical composition of molten steel. Therefore, the inclusion in the steel melt is consecutively modified during the refractory–slag–metal reactions assuming that the inclusion–metal reaction (R3) goes to equilibrium in each time step. The conceptual (schematic) illustration for the above reactions is shown in Figure 2. Even though the reaction between refractory and molten steel also causes Mg pick-up into the molten steel, the Mg pick-up originated from the refractory–metal reaction is significantly lower than that from the slag–metal reaction in view of kinetics.[10,30] Therefore, the

refractory–steel reaction was not considered in the present study.

In the present study, the so-called "Effective Equilibrium Reaction Zone (EERZ) Model" was adopted to predict the formation behavior of inclusion during the refractory–slag–metal reactions. The EERZ model concept has been used for the process simulations such as RH degassing,[14] continuous casting,[15] VOD,[13] and basic oxygen steelmaking processes.[17] In the EERZ model, all phases within the "effective reaction zone" located at the reaction interface are assumed to reach an equilibrium.[14]

The reaction zone mass per unit step is considered for describing the mass transfer in each phase, instead of the general flux density equations. That is, a constant mass of metal (V_M^t) from the bulk metal and a constant mass of slag (V_S^t) from the bulk slag enter the metal–slag reaction zone at a fixed time interval (Δt). The reaction zone volume per unit step for metal phase and slag phase (V_M^t and V_S^t) can be described as follows:

$$V_M^t = \frac{W_M^t}{\rho_M} = d_M \cdot A \cdot \Delta t, \quad [1]$$

$$V_S^t = \frac{W_S^t}{\rho_S} = d_S \cdot A \cdot \Delta t, \quad [2]$$

where the subscripts M and S represent metal phase and slag phase, respectively, W^t represents reaction zone mass per unit step (g), d represents effective reaction zone depth of each phase per time interval (m/s),

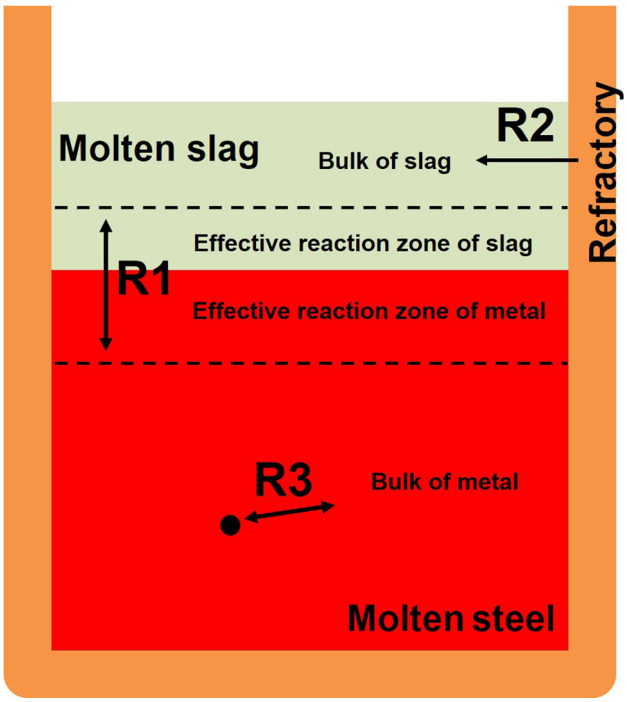

Fig. 2—Schematic representation of the slag–metal (R1), refractory–slag (R2), and inclusion–metal (R3) reactions in the present multiphase modeling system.

ρ represents density of each phase (g/m^3), and A represents the interface area between metal and slag phase (m^2).

Using EERZ model, one can calculate the multicomponent and multiphase equilibria by linking thermodynamic software. In the present study, the thermodynamic equilibrium at each reaction zone was calculated using FactSage^{TM} software (version 7.0).[31,32] The 'FTmisc' database was used for liquid steel.[33,34] The oxide solution such as slag and inclusion were calculated using 'FToxid' database, which has been developed including not only oxide system but also oxyfluoride system by the modified quasichemical model.[35–38] This software has been successfully employed to estimate the thermodynamic equilibria for the gas–slag–metal–refractory multiphase reactions in ferrous and nonferrous metallurgical systems.[39–50]

B. *Determination of Effective Reaction Zone Depth for Slag–Metal Reaction Kinetics*

It is highly important to determine the reaction zone volume per unit step for accurate modeling of slag–metal reaction kinetics. As shown in Eqs. [1] and [2], because the reaction zone volume per unit step is determined as a function of effective reaction zone depth, the kinetic experiment of desulfurization was separately conducted to determine the mass transfer coefficient in the metal and slag phases. Then the mass transfer coefficients were employed to deduce the value of effective reaction zone depth in each phase.

Figure 3 shows the variation of sulfur content in molten steel and slag against reaction time due to the desulfurization reaction. The sulfur content in the steel melt decreases, whereas sulfur content in the slag increases with the increasing reaction time. The desulfurization rate at the metal and the slag phase can be represented by Eqs. [3] and [4], respectively.

$$-\frac{\mathrm{d}[\text{pct S}]_b}{\mathrm{d}t} = k_M \cdot \frac{\rho_M \cdot A}{W_M} \cdot [[\text{pct S}]_b - [\text{pct S}]_i], \quad [3]$$

$$\frac{\mathrm{d}(\text{pct S})_b}{\mathrm{d}t} = k_S \cdot \frac{\rho_S \cdot A}{W_S} \cdot [(\text{pct S})_i - [(\text{pct S})_b], \quad [4]$$

where W_M and W_S represent total weight of metal and slag, respectively, and subscripts b and i represent bulk and interface of each phase, respectively. The sulfur contents in the metal and slag phase are represented as [pct S] and (pct S), respectively. The mass transfer coefficient in the metal and slag phase (k_M and k_S) can be obtained by considering the equilibrium distribution ratio of sulfur and its mass balance between slag and metal as follows:

$$-\left(\frac{[\text{pct S}]_0 - [\text{pct S}]_e}{[\text{pct S}]_0}\right) \cdot \frac{W_M}{\rho_M \cdot A} \cdot \ln\left[\frac{[\text{pct S}]_b - [\text{pct S}]_e}{[\text{pct S}]_0 - [\text{pct S}]_e}\right] = k_M \cdot t, \quad [5]$$

$$-\left(\frac{[\text{pct S}]_e}{[\text{pct S}]_0}\right)\cdot\frac{W_S}{\rho_S\cdot A}\cdot\ln\left[\frac{[\text{pct S}]_b-[\text{pct S}]_e}{[\text{pct S}]_0-[\text{pct S}]_e}\right]=k_S\cdot t, \quad [6]$$

Plotting the left-hand side of Eqs. [5] and [6] against reaction time provides a straight line with the slope equal to the k_M and k_S, respectively. In the present study, it was assumed that the equilibrium sulfur content, [pct S]$_e$, is equal to the sulfur content at 30 minutes. As a result, $k_M = 1.0 \times 10^{-4}$ m/s and $k_S = 3.5 \times 10^{-6}$ m/s were obtained, respectively, as shown in Figure 4.

The sulfur content in the metal phase at specific time t ([pct S]$_b^t$) can be calculated by substituting k_M into Eq. [5]. Alternatively, the sulfur content in the metal phase at specific time t can be determined by considering mass balance of sulfur and EERZ model concept (Eq. [7]) as follows:

$$[\text{pct S}]_b^t=\frac{[\text{pct S}]_0\cdot(W_M-W_M^t)+[\text{pct }S]_e\cdot W_M^t}{W_M}. \quad [7]$$

Rearranging Eq. [7], the effective reaction zone mass of metal phase per unit step can be obtained from Eq. [8]:

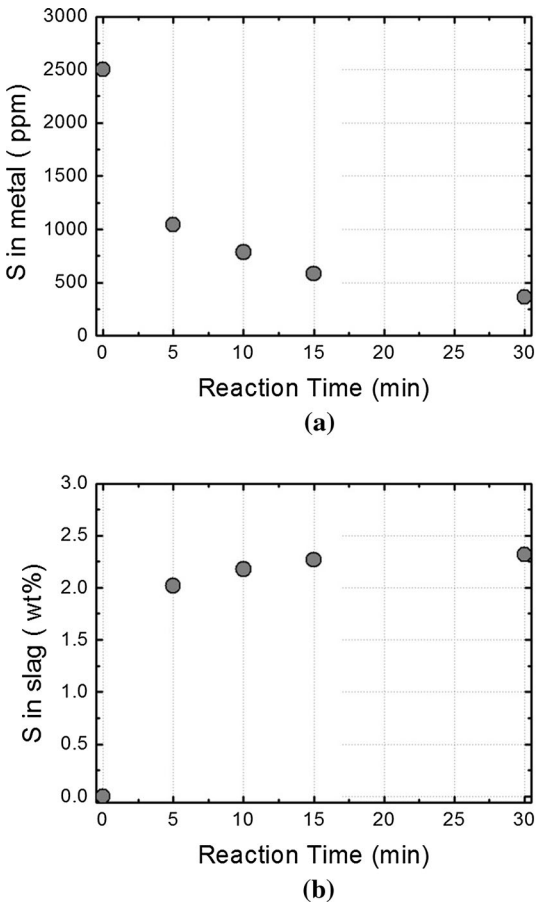

Fig. 3—Changes of sulfur content in the (*a*) metal phase and (*b*) slag phase at 1873 K (1600 °C).

$$W_M^t=\frac{([\text{pct S}]_b^t-[\text{pct S}]_0)}{([\text{pct S}]_e-[\text{pct S}]_0)}\cdot W_M. \quad [8]$$

Thus, the effective reaction zone depth of metal phase per unit time interval (d_M) can be calculated by combining k_M value and Eqs. [1], [5], and [8]. The effective reaction zone depth of slag phase per unit time interval (d_S) can be deduced in a similar way. Consequently, $d_M = 1.0 \times 10^{-4}$ m/s and $d_S = 2.5 \times 10^{-5}$ m/

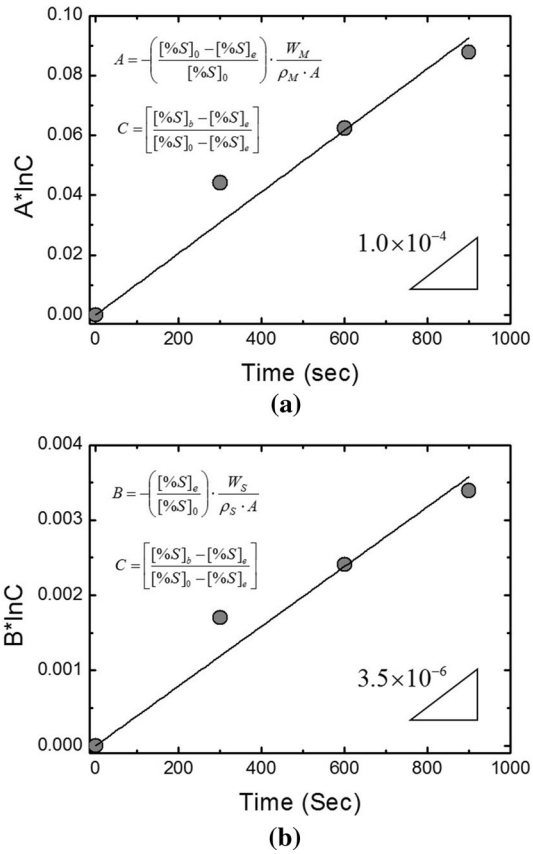

Fig. 4—Integrated kinetic plot for the mass transfer coefficient of sulfur in (*a*) metal and (*b*) slag phase at 1873 K (1600 °C).

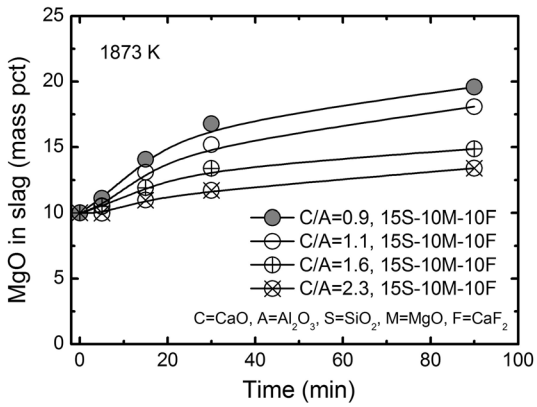

Fig. 5—Variation of MgO content in the slag during the slag–refractory reaction at 1873 K (1600 °C).

Table I. Mass Transfer Coefficient of MgO in the Slag at 1873 K (1600 °C)

Slag Composition				
C/A	SiO_2	MgO	CaF_2	k_{MgO} ($\times 10^6$ m/s)
0.9	15	10	10	4.9 (±0.20)
1.1	15	10	10	4.1 (±0.23)
1.6	15	10	10	4.7 (±0.26)
2.3	15	10	10	2.8 (±0.25)

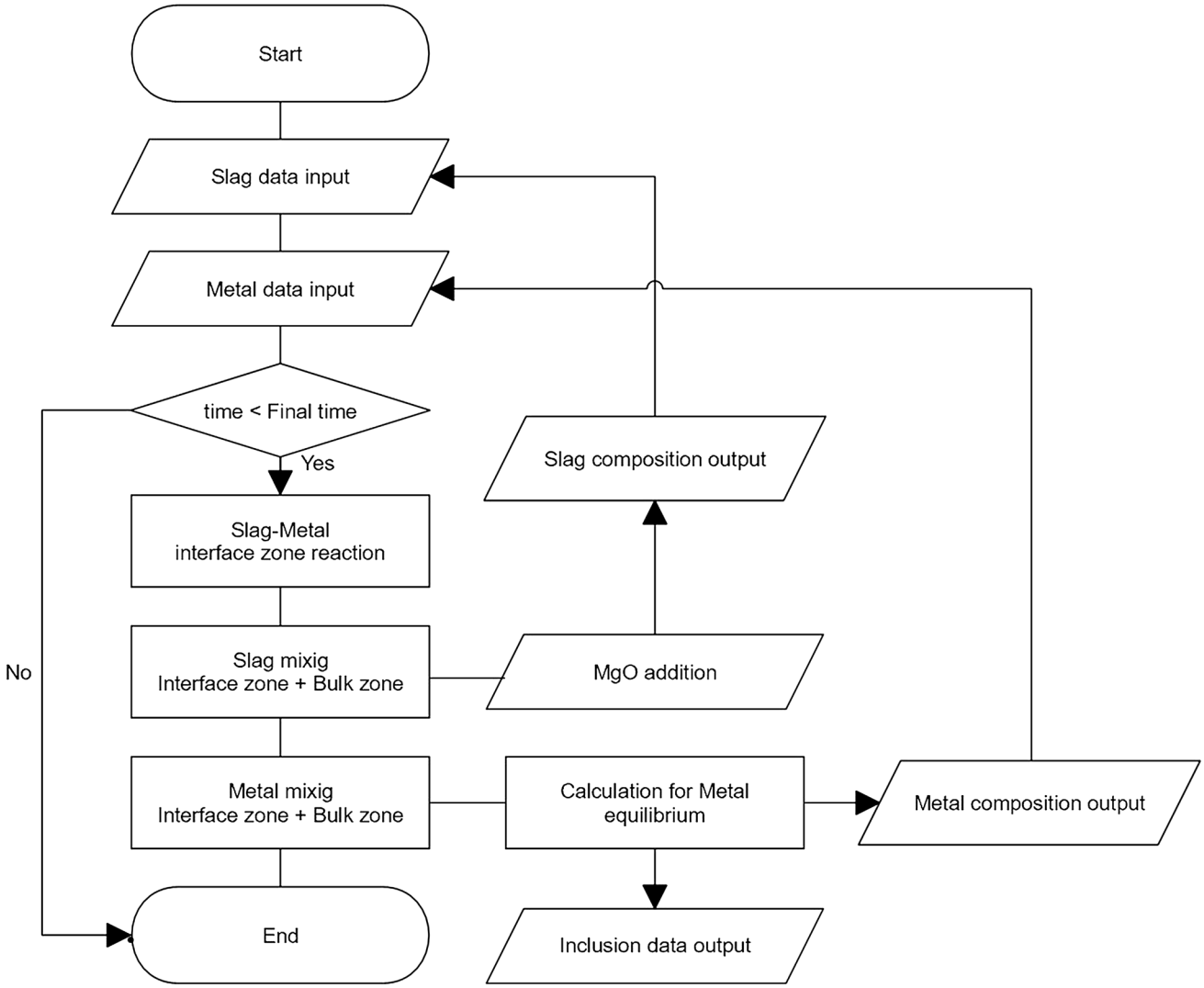

Fig. 6—Flow chart of the refractory–slag–metal–inclusion multiphase reactions modeling.

s were obtained, respectively, and these values were used to determine the reaction zone volume per unit step for metal and slag phase based on Eqs. [1] and [2].

C. *Dissolution Rate of Refractory into Slag Phase*

In the present study, the fused magnesia crucible was used as a refractory material, and thus, it was assumed that the mass transfer of MgO in the slag phase is a rate controlling step of the MgO dissolution process. Hence, the driving force of the dissolution of refractory is expressed by a difference between the saturation limit of MgO, $(\text{pct MgO})_{sat}$, and the actual MgO content in the slag at certain time t, $(\text{pct MgO})_t$. Then the rate equation of MgO dissolution is given as follows:

$$\frac{\mathrm{d}(\text{pct MgO})}{\mathrm{d}t} = k_{MgO} \cdot \frac{\rho_S \cdot A_{slag/ref}}{W_S} \cdot [(\text{pct MgO})_{sat} - (\text{pct MgO})_t], \quad [9]$$

where the k_{MgO} represents the mass transfer coefficient of MgO in the slag phase, and $A_{slag/ref}$ represents the

interfacial area between slag and refractory phase. The mass transfer coefficient of MgO (k_{MgO}) can be obtained by integrating Eq. [9] as follows:

$$-\ln\left[\frac{(\text{pct MgO})_{sat}-(\text{pct MgO})_t}{(\text{pct MgO})_{sat}-(\text{pct MgO})_0}\right]\cdot\left(\frac{W_S}{\rho_S\cdot A_{slag/ref}}\right)=k_{MgO}\cdot t, \quad [10a]$$

$$(\text{pct MgO})_t=(\text{pct MgO})_{sat}-\left[\exp\left(-\frac{\rho_S\cdot A_{slag/ref}}{W_S}\cdot k_{MgO}\cdot t\right)\cdot\left((\text{pct MgO})_{sat}-(\text{pct MgO})_0\right)\right], \quad [10b]$$

where the (pct MgO)$_0$ is the initial content of MgO in the slag. Here the actual MgO content in the slag at time t, (pct MgO)$_t$, in the present modeling is defined as

$$(\text{pct MgO})_t=\frac{W^t_{MgO}}{W^{t-1}_{S,total}+W^t_{MgO}}\times 100, \quad [11a]$$

$$W^t_{MgO}=\frac{(\text{pct MgO})_t}{100-(\text{pct MgO})_t}\cdot W^{t-1}_{S,total}, \quad [11b]$$

where W^t_{MgO} represents the mass of MgO in the slag at time t and $W^{t-1}_{S,total}$ represents the total mass of the slag at the right before certain time t. Combining Eqs. [10b] and [11b], W^t_{MgO} can be obtained.

Table II. Simulation Conditions

Parameters	Value (unit)
Weight of slag (W_S)	50 (g)
Weight of metal (W_M)	600 (g)
Diameter of crucible	50 (mm)
Density of molten steel	6.96 (g/cm^3)
Density of molten slag	2.50 (g/cm^3)
Temperature	1873 (K) (1600 °C)
Effective reaction zone depth of metal phase (d_M)	1.0×10^{-4} (m/s)
Effective reaction zone depth of slag phase (d_S)	2.5×10^{-5} (m/s)
Mass transfer coefficient of MgO (k_{MgO})	5.0×10^{-6} (m/s)
Time per unit step	60 (s)
Total number of steps	30
Total time	1800 (s)

The saturation limit of MgO, (pct MgO)$_{sat}$, of the present slag system was calculated using FactSage™7.0 software, and the $W^{t-1}_{S,total}$ could be obtained in the process of refractory–slag–metal reaction model at each step. Knowing the k_{MgO}, the MgO content in the slag at certain time t can be calculated. Therefore, the determination of k_{MgO} is highly important to construct the precise kinetic model for the slag–refractory reaction.

The changes of MgO content in the slag as a function of reaction time is shown in Figure 5. The MgO content increases with the increasing time due to dissolution of MgO from refractory to slag. The mass transfer coefficient of MgO (k_{MgO}) was calculated through Eq. [10a], and the results are presented in Table I. Umakoshi *et al.*[41] measured k_{MgO}, which ranges from 10^{-6} to 10^{-5} m/s, in the CaO-SiO$_2$-Fe$_t$O slag system at 1673 K (1400 °C) by rotating method. Vollmann and Harmuth obtained k_{MgO} = 10^{-6} to 10^{-3} m/s from the numerical simulation for the actual ladle operation conditions.[42] Therefore, in the present study, the mass transfer coefficient of MgO, k_{MgO} = 5.0×10^{-6} m/s, was adopted for the simulation of the refractory–slag–metal–inclusion multiphase reactions.

D. *Flow Chart of Refractory–Slag–Metal–Inclusion Multiphase Reactions Modeling*

A flow chart of the refractory–slag–metal–inclusion multiphase reactions modeling is shown in Figure 6. At first, the process variables such as total amount of slag and metal, temperature, mass transfer coefficient, and size of ladle (data are presented in Table II) are

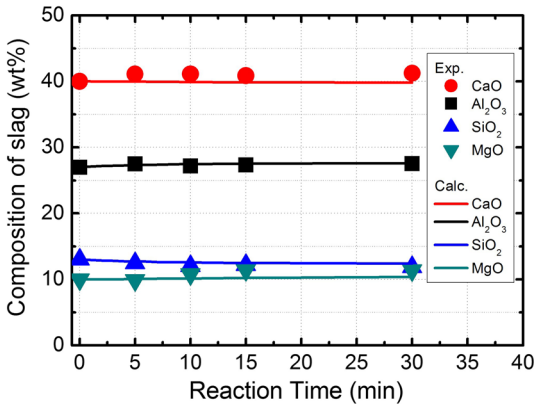

Fig. 7—Calculated and measured results of the slag composition at 1873 K (1600 °C).

Table III. Initial Composition of Slag and Metal for the Refractory–Slag–Metal–Inclusion Multiphase Reactions Modeling

	Slag Composition (Mass Pct)					
	CaO	Al_2O_3	SiO_2	MgO	CaF_2	Metal Composition (Mass Pct)
Case 1	40	33	7	10	10	Fe-0.8Mn-0.4Si-0.05Al-0.3C-0.004O
Case 2*	40	27	13	10	10	Fe-0.8Mn-0.4Si-0.05Al-0.3C-0.004O
Case 3	40	21	19	10	10	Fe-0.8Mn-0.4Si-0.05Al-0.3C-0.004O

*Compared with experimental data in Section IV-A.

inputted. The initial metal and slag compositions are presented in Table III. Then the slag–metal reaction at the EERZ is calculated, at which the reaction volumes of metal and slag phase are calculated using Eqs. [1] and [2].

Next, the EERZ of slag and bulk slag is mixed for the homogenization of the slag phase, from which the value of total amount of slag ($W^{t-1}_{S,total}$) is deduced for the calculation of the increase in MgO amount to describe the MgO dissolution from the refractory using Eqs. [10] and [11]. This result is inputted to the equilibrium calculation of slag phase, from which the slag composition at certain time t is obtained. Simultaneously, the EERZ of metal and bulk metal is mixed for the homogenization of the metal phase, from which the composition of molten steel at certain time t, and thus, the inclusion information can be finally obtained. During this intermixing calculation, it is assumed that the amount of inclusions removed by floating at each time step is equal to the ratio of the effective zone mass to the total mass of metal phase, *i.e.*, W^t_M/W_M. This procedure is one step of the calculation, and the above procedure is repeated until time t is a satisfied final time. The calculated compositions of slag and metal phase at one step are used as the initial variables for the next step calculation.

IV. RESULTS AND DISCUSSION

A. *Comparison Between Experimental Data and Modeling Results for Refractory–Slag–Metal–Inclusion Multiphase Reactions*

The changes in the composition of molten slag and molten steel are shown in Figures 7 and 8, respectively. The experimental results of the concentrations of magnesium and calcium could not be obtained due to difficulty in chemical analysis. The calculated results for the slag and molten steel are in good agreement with the experimental results. The aluminum content in the steel melt gradually decreases as the slag–metal reaction proceeds, while the silicon content slightly increases. This tendency is clearly observed from both experimental and calculation results and originated from the reduction of SiO_2 in the slag by Al in molten steel as given in the following equation:

$$3(SiO_2) + 4[Al] = 3[Si] + 2(Al_2O_3). \quad [12]$$

The calculated concentration of Mg in molten steel gradually increases at the early stage of the reaction, whereas an incubation time delay (approximately 5 minutes) for an increase in Ca concentration is predicted. This possibly originated from the fact that the activity of MgO is close to unity, while that of CaO is

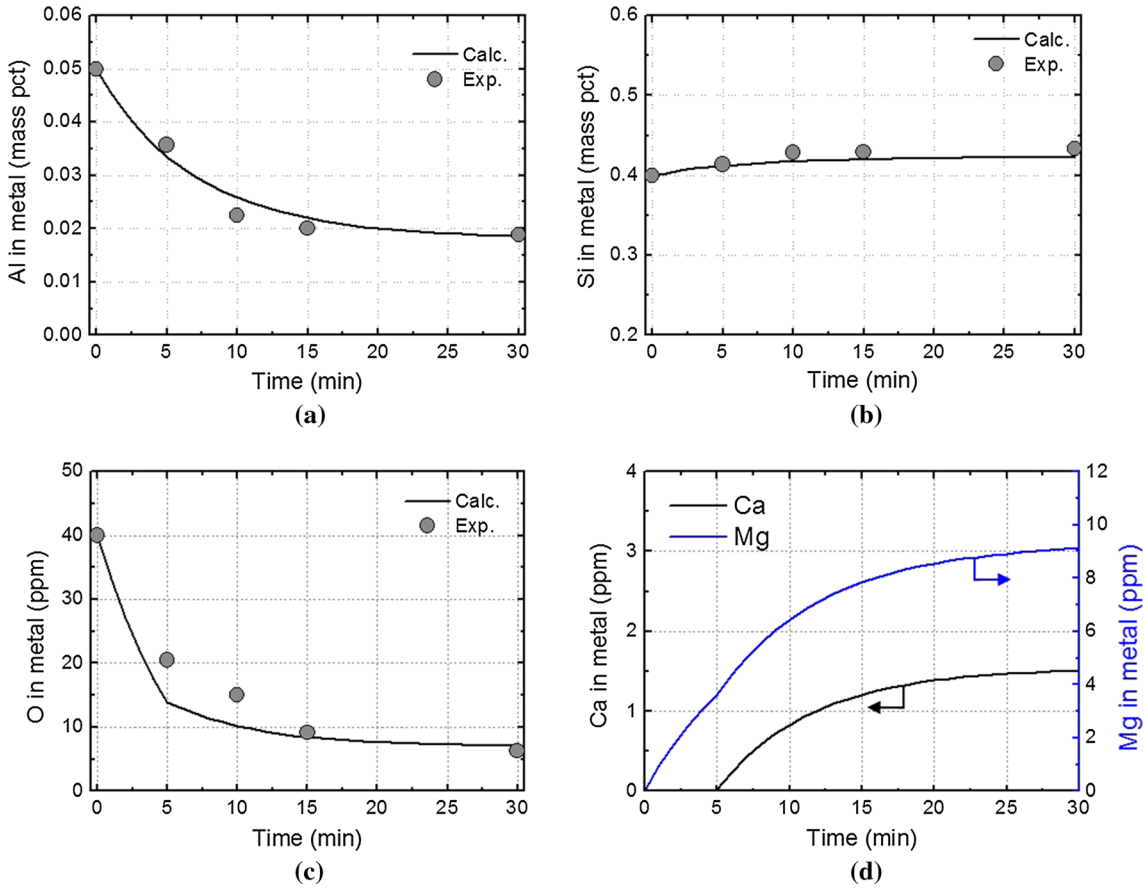

Fig. 8—Calculated and measured results of the composition of molten steel: (*a*) aluminum, (*b*) silicon, (*c*) oxygen, and (*d*) calcium and magnesium at 1873 K (1600 °C).

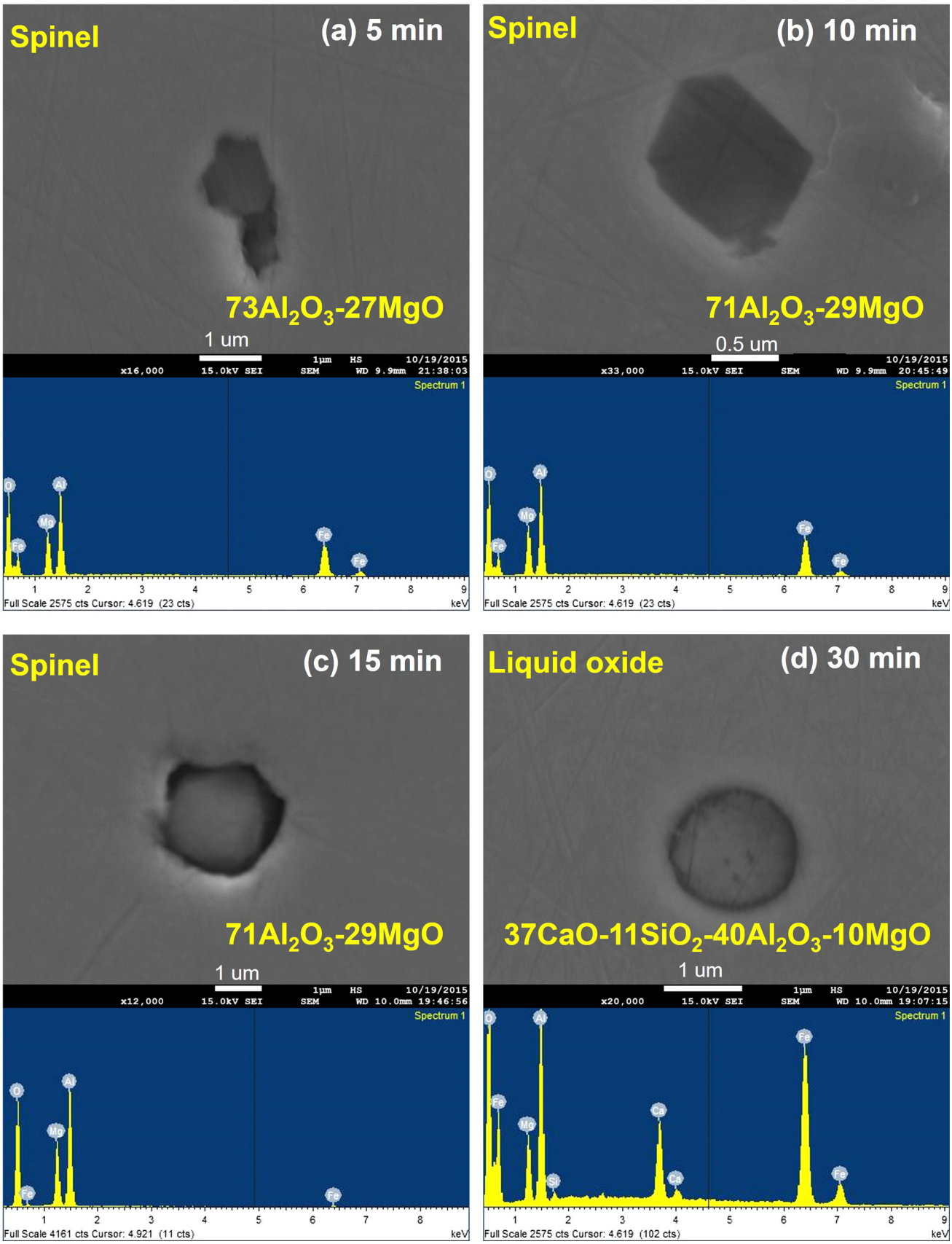

Fig. 9—SEM images of the typical inclusions observed at (*a*) 5 min, (*b*) 10 min, (*c*) 15 min, and (*d*) 30 min at 1873 K (1600 °C) (numbers are mass pct of each oxide).

much lower than unity in the initial slag phase. The more detailed discussion will be given in the following section, *i.e.*, section IV-B (Figure 14). The Mg and Ca pick-up due to slag–metal reaction is given as follows, respectively:[10]

$$3(MgO) + 2[Al] = 3[Mg] + (Al_2O_3), \quad [13]$$

$$3(CaO) + 2[Al] = 3[Ca] + (Al_2O_3). \quad [14]$$

As shown in Figure 8, it is very interesting that the calculated content of oxygen shows a change in slope at a time of 5 minutes (Figure 8(c)), which can be understood from the tendencies of Mg and Ca pick-up reactions given in Eqs. [13] and [14] as well as shown in Figure 8(d). At 5 minutes after Al was added, Al was additionally consumed by the reaction with CaO (Eq. [14]), resulting in a decrease in effective Al to react with oxygen. Thus, the oxygen removal rate decreased at a time of 5 minutes.

The SEM images of typical inclusions observed in molten steel at each reaction time, *i.e.*, 5, 10, 15, and 30 minutes, are shown in Figure 9. The $MgAl_2O_4$ spinel inclusion was observed at the early to middle stage of the reaction, viz. within 15 minutes. However, the liquid oxide inclusion consisted of the CaO-Al_2O_3-SiO_2-MgO system was mainly observed at the final stage of the reaction (30 minutes). The inclusions were classified to alumina, spinel, and liquid oxide in the present study.

The variation of the relative fraction (population) of each type of inclusion is represented as a function of reaction time in Figure 10. The initial inclusion was alumina, which originated from the Al deoxidation reaction. After 5 minutes since Al was added, the alumina inclusion transformed to spinel, of which fraction is greater than about 90 pct and the relative fraction of the liquid oxide inclusion slightly increased. Finally, the fraction of the liquid oxide inclusion increased to about 2/3 of the total inclusion.

The change in the relative inclusion fraction during the slag–metal reaction was calculated and is shown in Figure 11. It is very interesting that the calculation results represent the qualitatively similar tendency of the inclusion evolution process to those obtained in the experiments (Figure 10). Alumina inclusion gradually disappears, while the spinel becomes major inclusion since 5 minutes after Al addition, resulting from the fact that alumina inclusion transforms to spinel by Eqs. [13] and [15]:[10]

$$4(Al_2O_3)_{inclusion} + 3[Mg] = 3(MgO \cdot Al_2O_3)_{inclusion} + 2[Al]. \quad [15]$$

Afterward, the relative fraction of liquid oxide gradually increases, indicating that the spinel inclusion is continuously modified to the liquid oxide due to the reaction with calcium (Eq. 16) transferred from slag to metal phase (Eq. [14]). Simultaneously, a reduction of SiO_2 in the slag is continuously occurred by Al in molten steel, which provides Si transfer from slag to metal phase (Eq. [12]). Thus, a dissolved Si reacts with MgO-Al_2O_3 (-CaO) inclusions by Eq. [17]:

$$[Ca] + \left(x + \frac{1}{3}\right)(yMgO \cdot Al_2O_3)_{inclusion} = \left(CaO \cdot xAl_2O_3 \cdot y\left(x + \frac{1}{3}\right)MgO\right)_{inclusion} + \frac{2}{3}[Al], \quad [16]$$

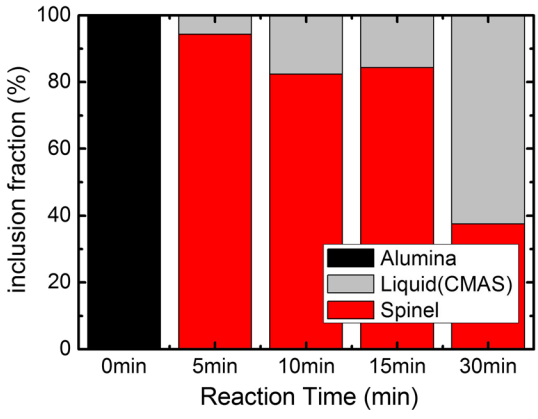

Fig. 10—Experimental results for the change in the relative fraction (population) of the inclusions in molten steel at 1873 K (1600 °C).

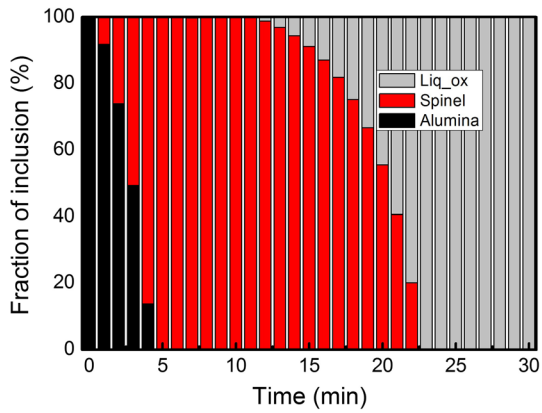

Fig. 11—Calculated results for the change in the relative fraction (population) of the inclusions in molten steel at 1873 K (1600 °C).

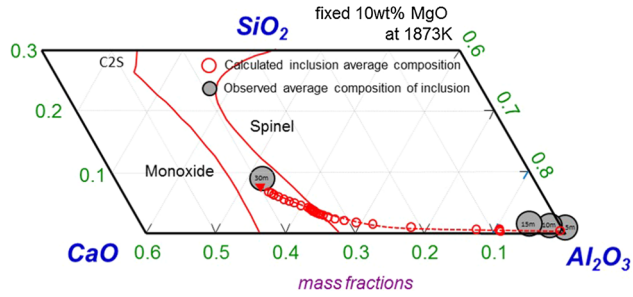

Fig. 12—Trajectory of the composition of the inclusions in molten steel reacted with ladle slag at 1873 K (1600 °C) (phase diagram was calculated by FactSage™7.0).

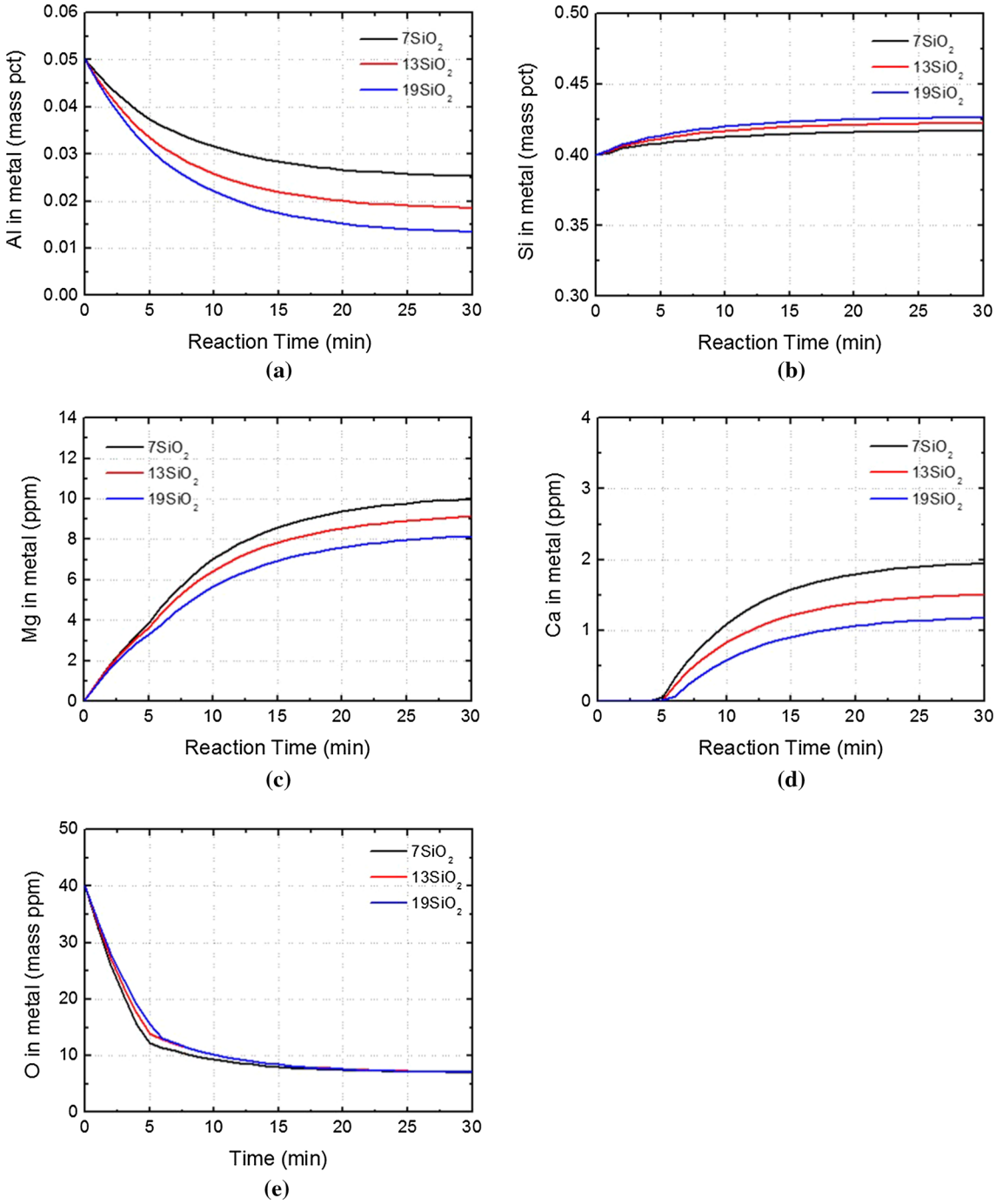

Fig. 13—Predicted results of the composition of molten steel reacted with ladle slag at different SiO_2 level; (*a*) aluminum, (*b*) silicon, (*c*) magnesium, (*d*) calcium, and (*e*) oxygen at 1873 K (1600 °C).

$$[\mathrm{Si}] + \left(x + \frac{2}{3}\right)(y\mathrm{MgO} \cdot \mathrm{Al_2O_3})_{\mathrm{inclusion}} = \left(\mathrm{SiO_2} \cdot x\mathrm{Al_2O_3} \cdot y\left(x + \frac{2}{3}\right)\mathrm{MgO}\right)_{\mathrm{inclusion}} + \frac{4}{3}[\mathrm{Al}]. \quad [17]$$

Consequently, the spinel inclusion is predicted to be entirely modified to the $CaO\text{-}Al_2O_3\text{-}MgO\text{-}SiO_2$ liquid oxide inclusion at 23 minutes.

The trajectory of the average composition of the inclusions is plotted in the $CaO\text{-}Al_2O_3\text{-}SiO_2$-10 mass pct MgO phase diagram at 1873 K (1600 °C) in Figure 12. The predicted inclusion evolution path is also appeared for the sake of comparison. The calculated inclusion trajectory is in good agreement with the experimental observations. As shown in Figure 12, the content of CaO sharply increases, and the SiO_2 content increases mildly with the increasing reaction time, while the content of Al_2O_3 in the inclusion drastically decreases.

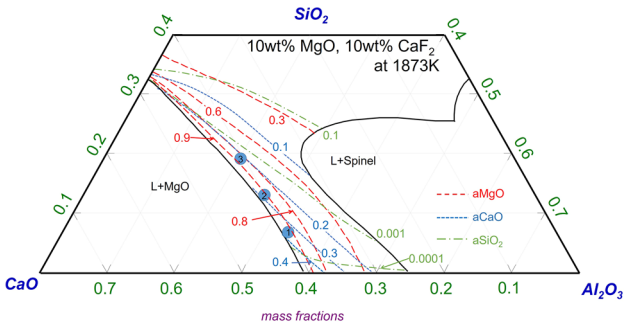

Fig. 14—Iso-activity contours of MgO, CaO, and SiO_2 in the $CaO-Al_2O_3-SiO_2$-10MgO-10CaF_2 system at 1873 K (1600 °C) (calculated by FactSage™7.0).

Even though there is slight difference between the calculated and measured results, the refractory–slag–metal multiphase reaction model constructed in the present study exhibits a good predictability of the inclusion evolution during ladle refining process.

B. *Applications of Refractory–Slag–Metal–Inclusion Multiphase Reaction Model: Effect of Silica Content in Ladle Slag on Inclusion Evolution Process*

The initial SiO_2 content in the ladle slag was varied as presented in Table III to evaluate the effect of slag composition, viz. SiO_2 content on the evolution behavior of the inclusions in molten steel based on the present refractory–slag–metal–inclusion multiphase reaction model. Other conditions are all the same as shown in Table II. The change in the steel composition with reaction time calculated by the present model is shown in Figure 13. The aluminum content gradually decreases during the slag–metal reaction, while the silicon content slightly increases based on Eq. [12]. The higher the content of SiO_2 in the slag, the lower the Al content remained in molten steel. This is because the activity of SiO_2 in the slag increases from about 10^{-4} to 10^{-3} when the SiO_2 content increases from 7 to 19 mass pct as shown in Figure 14. The content of magnesium and calcium also gradually increases with reaction time, and the lower the residual contents are expected as the content of SiO_2 increases. This originated from the fact that the activity of MgO and CaO slightly decreases with the increasing SiO_2 content in the slag.

The changes in the relative fraction of each type of inclusion at different SiO_2 content are shown in Figure 15. As the content of SiO_2 in the slag increases from 7 to 19 mass pct, the starting point of the modification of spinel into the liquid oxide is delayed from about 9 to 20 minutes, and the finishing point of the modification reaction follows the same tendency. The trajectory of the calculated composition of the inclusions is plotted in the $CaO-Al_2O_3-SiO_2$-10 mass pct MgO phase diagram at 1873 K (1600 °C) in Figure 16. The content of CaO sharply increases and the SiO_2 content increases with the increasing reaction time, while the content of Al_2O_3 in the inclusion drastically decreases. Therefore, the $CaO-Al_2O_3-SiO_2-MgO$ system liquid inclusion is formed at the final stage of the

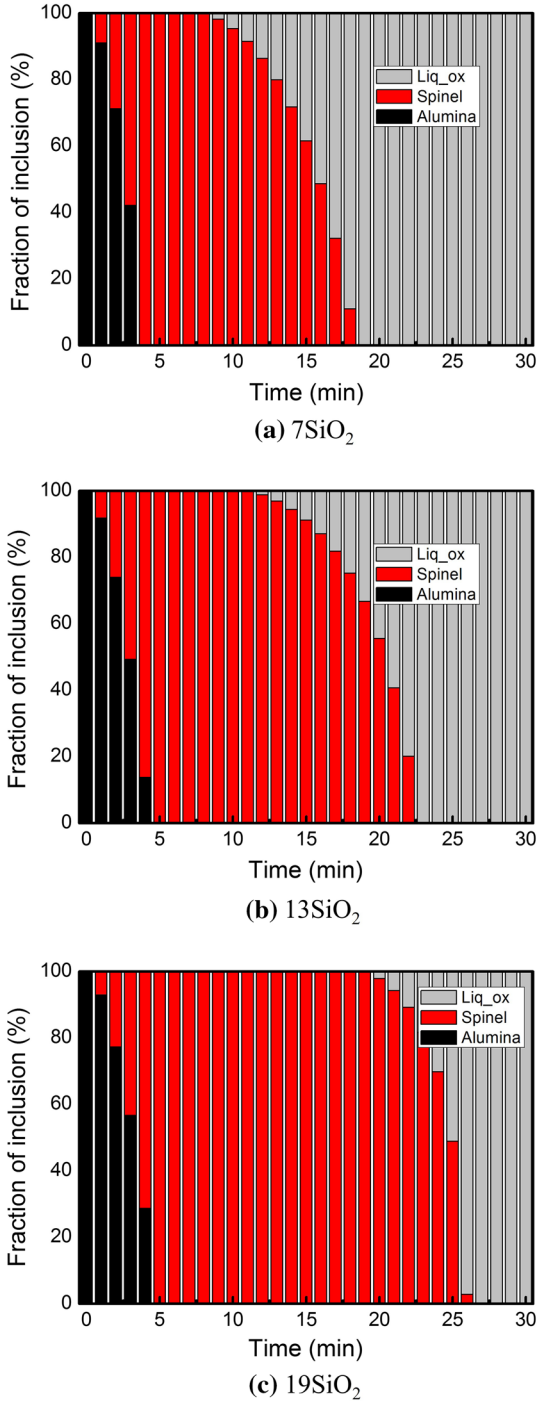

Fig. 15—Calculated results for the change in the relative fraction (population) of the inclusions in molten steel reacted with ladle slag of which silica content is (*a*) 7, (*b*) 13, and (*c*) 19 mass pct at 1873 K (1600 °C).

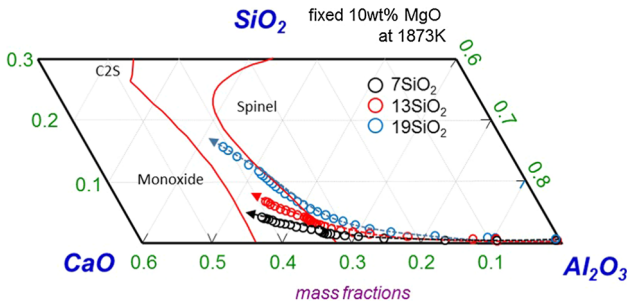

Fig. 16—Trajectory of the predicted composition of the inclusions in molten steel reacted with ladle slag at different silica contents at 1873 K (1600 °C) (phase diagram was calculated by FactSage™7.0).

reaction. The increase of the SiO_2 content in the inclusions is more significant when the SiO_2 content in the slag is 19 mass pct at a given reaction time, *i.e.*, 30 minutes.

V. CONCLUSIONS

The refractory–slag–metal–inclusion multiphase reaction model was developed by integrating the refractory–slag, slag–metal, and metal–inclusion elementary reactions in order to predict the evolution of inclusions during the secondary refining processes. The mass transfer coefficient in the metal and slag phase, and the mass transfer coefficient of MgO in the slag were employed in the present multiphase reactions modeling. The major findings of the present study are as follows:

(1) The "Effective Equilibrium Reaction Zone (EERZ) Model" was basically employed for the refractory–slag–metal–inclusion multiphase reactions modeling. The reaction zone volume per unit step for metal and slag phase, which is dependent on the effective reaction zone depth in each phase, should be defined. Thus, we calculated the effective reaction zone depth in metal and slag phase per unit time interval ($d_M = 1.0 \times 10^{-4}$ m/s and $d_S = 2.5 \times 10^{-5}$ m/s) using the mass transfer coefficient of sulfur in each phase, which was measured in the present study.
(2) Because the dissolution rate of MgO from the refractory to slag phase is one of the key factors affecting the slag composition, the mass transfer coefficient of MgO in the ladle slag was also experimentally determined at 1873 K (1600 °C), *i.e.*, $k_{MgO} = 5.0 \times 10^{-6}$ *m/s*.
(3) The calculated results for the variation of the composition of slag and molten steel as a function of reaction time were in good agreement with the experimental results. The aluminum content in the steel melt gradually decreases as the slag–metal reaction proceeds, while the silicon content slightly increases. The calculated concentration of magnesium and calcium in molten steel gradually increase at the early stage of the reaction.
(4) The $MgAl_2O_4$ spinel inclusion was observed at the early to middle stage of the reaction, viz. within 15 minutes, whereas the liquid oxide inclusion was mainly observed at the final stage of the reaction (30 minutes). The content of CaO sharply increased, and the SiO_2 content increased mildly with the increasing reaction time, while the content of Al_2O_3 in the inclusion drastically decreased. Even though there are slight difference between the calculated and measured results, the refractory–slag–metal multiphase reaction model constructed in the present study exhibited a good predictability of the inclusion evolution during ladle refining process.

ACKNOWLEDGMENT

The present authors express great thanks to Professor In-Ho Jung, McGill University, Canada, for his help for using thermodynamic database, which is significantly important in the present refractory–slag–metal–inclusion multiphase reactions modeling with the FactSage™ software package.

REFERENCES

1. E. Sunami, S. Nozaki, Y. Tamaou, and T. Miura: *Tetsu-to-Haganė*, 1982, vol. 68, p. S248.
2. O. Suzuki, M. Oguchi, K. Nohara, T. Emi, and T. Mihara: *Tetsu-to-haganė*., 1982, vol. 68, p. S249.
3. M. Hojo, R. Nakao, T. Umezaki, H. Kawai, S. Tanaka, and S. Fukumoto: *ISIJ Int*., 1996, vol. 36, pp. S128–31.
4. H. Todoroki and K. Mizno: *ISIJ. Int*., 2004, vol. 44, pp. 1350–57.
5. J.H. Park and D.S. Kim: *Metall. Mater. Trans. B*, 2004, vol. 36B, pp. 495–97.
6. J.H. Park and Y.B. Kang: *Metall. Mater. Trans. B*, 2006, vol. 37B, pp. 791–98.
7. J.H. Park: *Calphad*, 2007, vol. 31, pp. 428–37.
8. J.H. Park: *Metall. Mater. Trans. B*, 2007, vol. 38B, pp. 657–63.
9. J.H. Park: *Mater. Sci. Eng. A*, 2007, vol. 472, pp. 43–51.
10. J.H. Park and H. Todoroki: *ISIJ. Int*., 2010, vol. 50, pp. 1333–46.
11. M. Jiang, X.H. Wang, and W.J. Wang: *Steel Res. Int*., 2010, vol. 81, pp. 759–65.
12. N. Verma, P.C. Pistorius, R.J. Fruehan, M. Potter, M. Lind, and S. Story: *Metall. Mater. Trans. B*, 2011, vol. 42B, pp. 711–19.
13. N. Verma, P.C. Pistorius, R.J. Fruehan, M. Potter, M. Lind, and S. Story: *Metall. Mater. Trans. B*, 2011, vol. 42B, pp. 720–29.
14. N. Verma, P.C. Pistorius, R.J. Fruehan, M.S. Potter, H.G. Oltmann, and E.B. Pretorius: *Metall. Mater. Trans. B*, 2012, vol. 43B, pp. 830–40.
15. Z. Deng and M. Zhu: *ISIJ. Int*., 2013, vol. 53, pp. 450–58.
16. R. Ding, B. Blanpain, P.T. Jones, and P. Wollants: *Metall. Mater. Trans. B*, 2000, vol. 31B, pp. 197–206.
17. M.A. Van Ende, Y.M. Kim, M.K. Cho, J. Choi, and I.H. Jung: *Metall. Mater. Trans. B*, 2011, vol. 42B, pp. 477–89.
18. M.A. Van Ende and I.H. Jung: *ISIJ. Int*., 2014, vol. 54, pp. 489–95.
19. D. Roy, P.C. Pistorius, and R.J. Fruhan: *Metall. Mater. Trans. B*, 2013, vol. 44B, pp. 1086–94.
20. D. Roy, P.C. Pistorius, and R.J. Fruhan: *Metall. Mater. Trans. B*, 2013, vol. 44B, pp. 1095–1104.
21. M. S. Kim: Reaction mechanism and kinetic analysis of chemical reactions between high Mn-high Al steel and CaO-SiO_2 type mold flux, PhD thesis, GIFT, POSTECH, Feb. 2016.
22. Y.S. Heish, Y. Watanabe, S. Asai, and I. Muchi: *Tetsu-to-Haganė*., 1983, vol. 69, pp. 596–603.

23. R.D. Morales and M. Macias-Hernandez: *Proc. AISTech 2011*, 2–5 May 2011, Indianapolis, IN, AIST, Warrendale, PA 15086, 2011, pp. 1339–56.
24. K.J. Graham and G.A. Irons: *Proc. SCANMET III*, 8–11 June 2008, Luleå, Sweden, MEFOS, Luleå, Sweden, 2008, vol. 1, pp. 385–96.
25. A. Galinodo, G.A. Irons, S. Sun and K. Coley: *Proc. CTSSC-EMI 2015*, 3–4 September 2015, Tokyo, Japan, 2015, pp. 22–31.
26. A. Harada, N. Maruoka, H. Shibata, and S.Y. Kitamura: *ISIJ. Int*., 2013, vol. 53, pp. 2110–17.
27. A. Harada, N. Maruoka, H. Shibata, and S.Y. Kitamura: *ISIJ. Int*., 2013, vol. 53, pp. 2118–25.
28. A. Harada, N. Maruoka, H. Shibata, M. Zeze, N. Asahara, F. Huang, and S.Y. Kitamura: *ISIJ. Int*., 2014, vol. 54, pp. 2569–77.
29. P.R. Scheller and Q. Shu: *Steel Res. Int*., 2014, vol. 85, pp. 1310–16.
30. A. Harada, G. Miyano, N. Maruoka, H. Shibata, and S.Y. Kitamura: *ISIJ. Int*, 2014, vol. 54, pp. 2230–38.
31. www.factsage.com (accessed December 2015).
32. C.W. Bale, E. Belisle, S.A. Decterov, G. Eriksson, K. Hack, I.H. Jung, Y.B. Kang, J. Melancon, A.D. Pelton, C. Robelin, and S. Petersen: *Calphad*, 2009, vol. 33, pp. 295–311.
33. A.D. Pelton: *Metall. Mater. Trans. B*, 1997, vol. 28B, pp. 869–76.
34. I.H. Jung, S.A. Decterov, and A.D. Pelton: *Metall. Mater. Trans. B*, 2004, vol. 35B, pp. 493–507.
35. I.H. Jung: *Proc. 4th Asia Steel Int. Conf*., 24–27 May 2009, Busan, Korea, KIM^{+}, Seoul, Korea, 2009, CR-ROM paper no. S3-30.
36. I.H. Jung: *Proc. AISTech 2010,* 3–6 May 2010, Pittsburgh, PA, AIST, Warrendale, PA 15086, 2010, pp. 1211–20.
37. I.H. Jung, M.A. Van Ende and D.G. Kim: *Proc. UNITECR 2011,* 30 October–2 November 2011, Kyoto, Japan, TARJ, Tokyo, Japan, 2011, pp. 582.
38. D.G. Kim, M.A. Van Ende, C. Van Hoek, C. Liebske, S. Van Der Laan, and I.H. Jung: *Metall. Mater. Trans. B*, 2012, vol. 43, pp. 1315–25.
39. Y.S. Han, D.R. Swinbourne, and J.H. Park: *Metall. Mater. Trans. B*, 2015, vol. 46B, pp. 2449–57.
40. S.K. Kwon, J.S. Park, and J.H. Park: *ISIJ Int*., 2015, vol. 55, pp. 2589–96.
41. J.S. Park, D.H. Kim, and J.H. Park: *J. Am. Ceram. Soc*., 2015, vol. 98, pp. 1974–81.
42. Y.S. Han and J.H. Park: *Metall. Mater. Trans. B*, 2015, vol. 46B, pp. 235–42.
43. S.K. Kwon, Y.M. Kong, and J.H. Park: *Metal. Mater. Int*., 2014, vol. 20, pp. 959–66.
44. J.S. Park and J.H. Park: *Steel Res. Int*., 2014, vol. 85, pp. 1303–09.
45. J.S. Park and J.H. Park: *Metall. Mater. Trans. B*, 2014, vol. 45B, pp. 953–60.
46. J.H. Shin and J.H. Park: *ISIJ Int*., 2013, vol. 53, pp. 2266–68.
47. J.H. Heo, B.S. Kim, and J.H. Park: *Metall. Mater. Trans. B*, 2013, vol. 44B, pp. 1352–63.
48. J.H. Park: *Metall. Mater. Trans. B*, 2013, vol. 44B, pp. 938–47.
49. M. Umakoshi, K. Mori, and Y. Kwai: *Tetsu-to-Haganė*., 1981, vol. 67, pp. 1726–34.
50. S. Vollmann and H. Harmuth: *Interceram*, 2012, vol. 61, pp. 19–21.